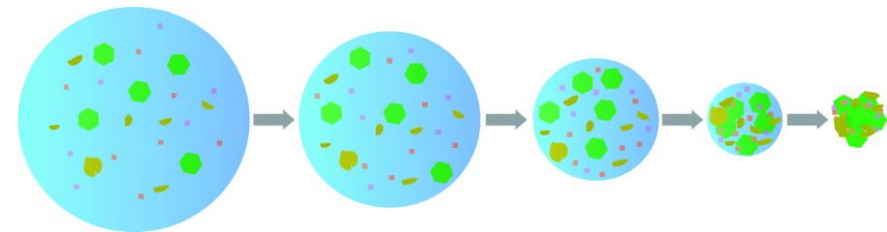
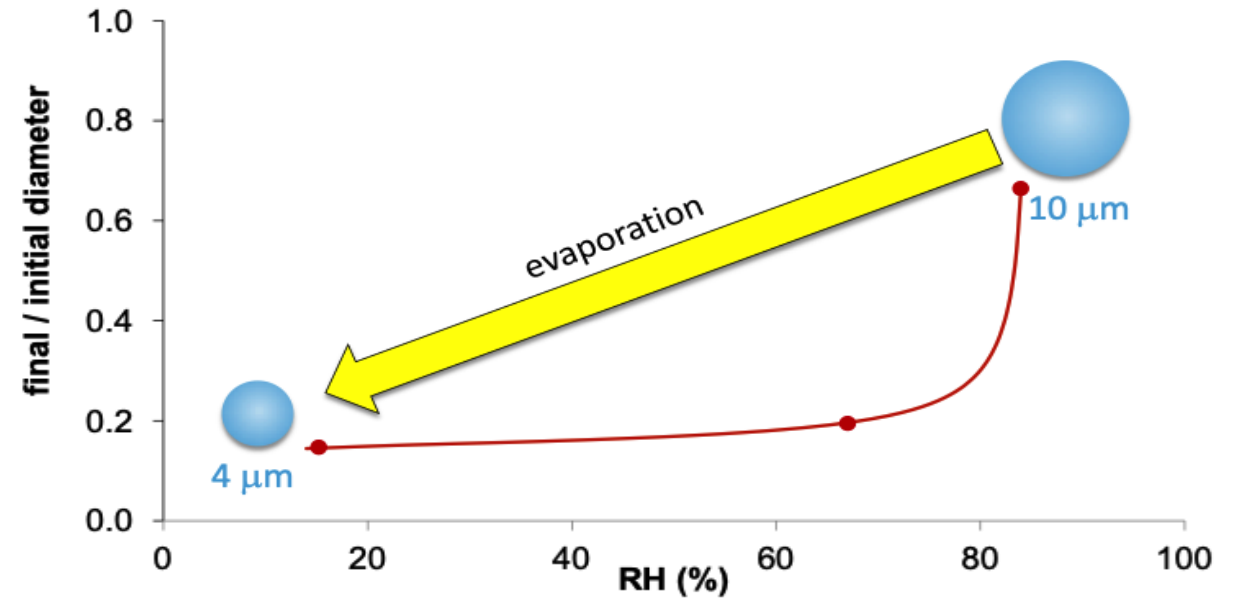
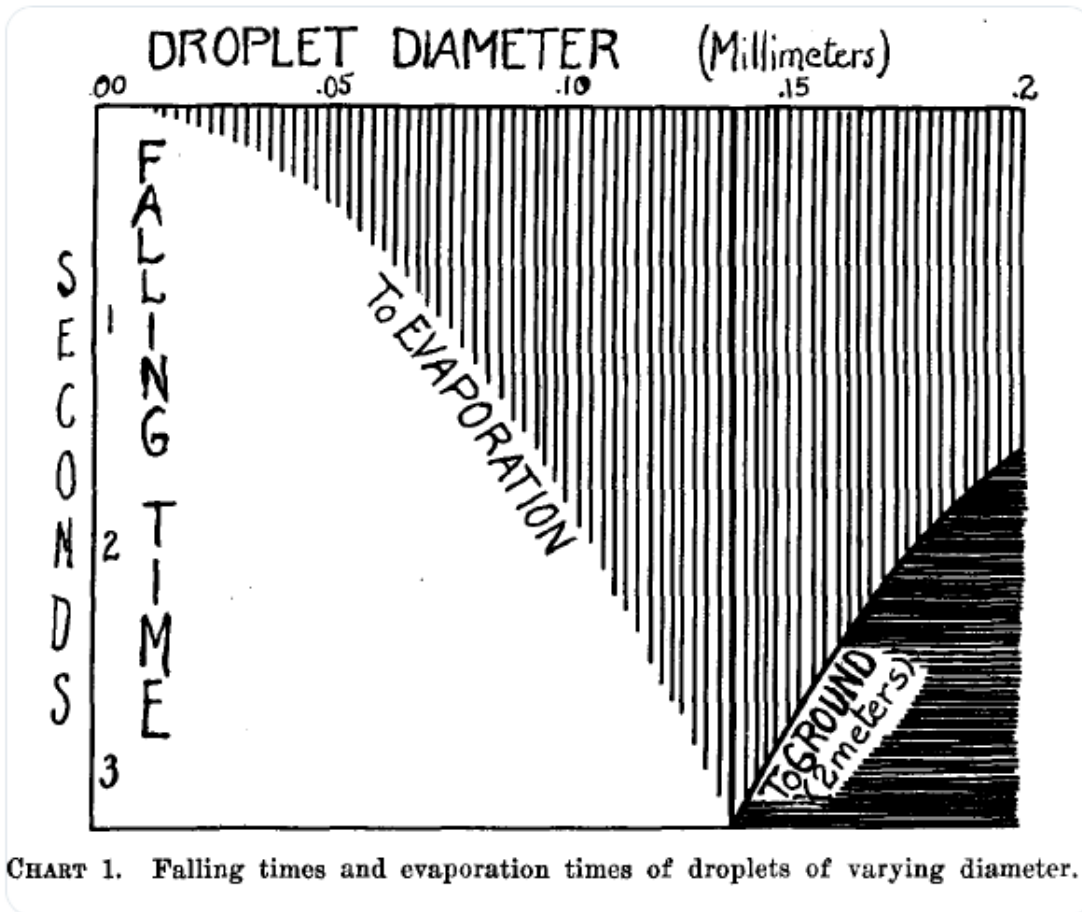


Fate in the air of respiratory particles





In the 1930s, William Wells (1886–1963), an environmental engineer, and his wife Milfred began applying more modern methods to the study of airborne transmission, particularly TB and measles. Droplets larger than 100 microns tend to fall (subject to gravity) before evaporating, while smaller droplets evaporate before falling. However, Wells encountered much resistance and was accused of trying to bring the miasma theory back into vogue.



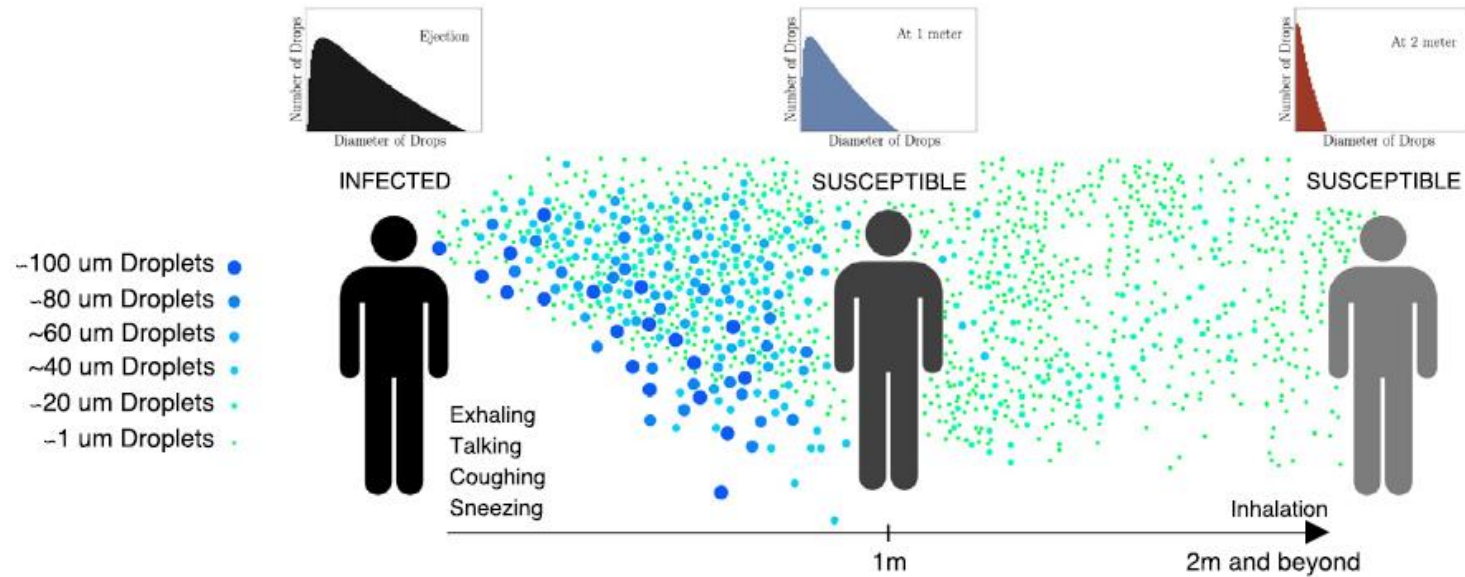
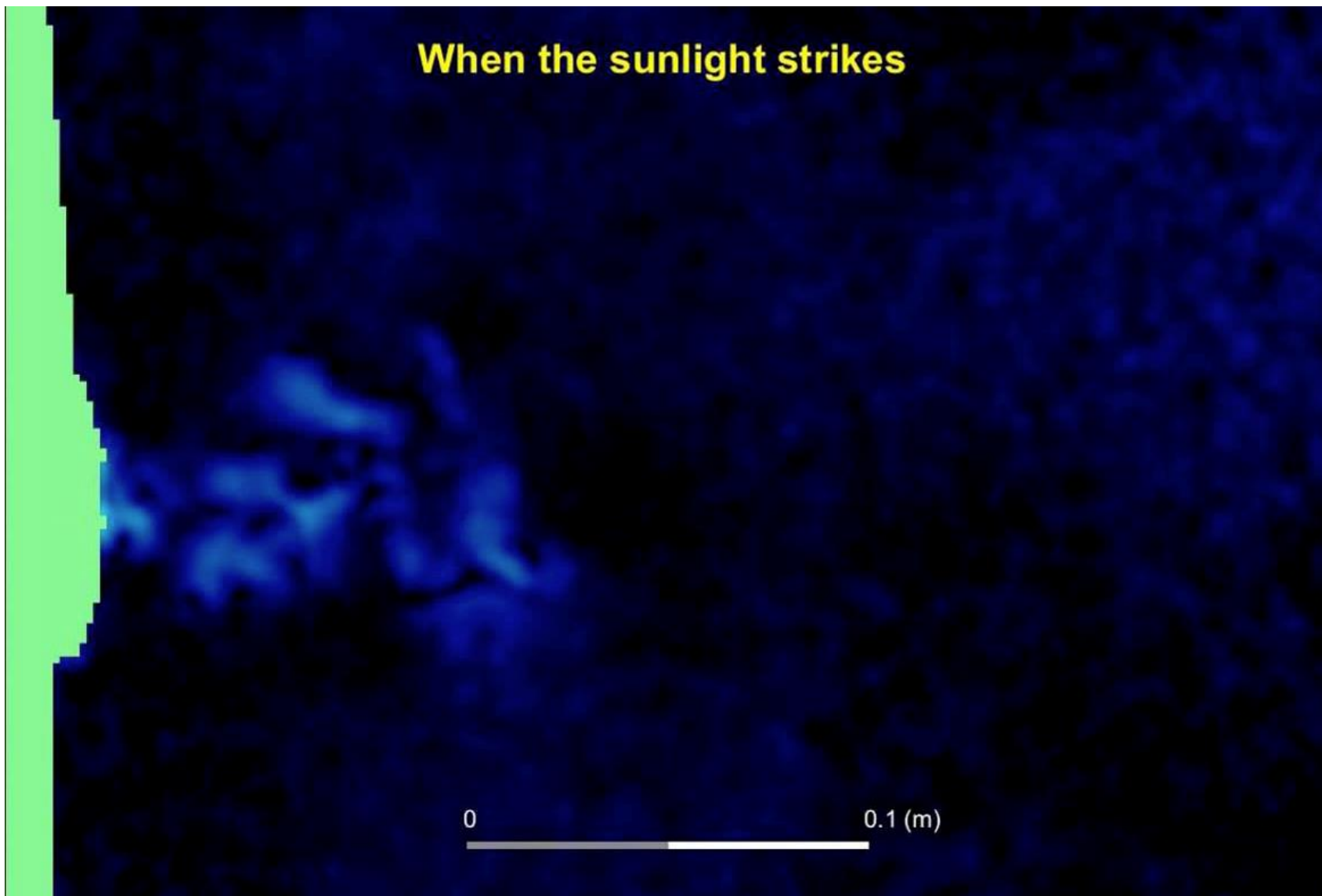


Fig. 2. The two dominant transmission routes (a) direct transmission route through ballistic larger droplets (b) indirect airborne transmission route by smaller airborne droplets and droplet nuclei. A schematic representation of size distribution at the infected source host, at an intermediate distance and at a receiving host located farther away is also shown.

When the sunlight strikes



- Puff: Warm, moist air exhaled during breathing, talking, coughing or sneezing, which remains coherent and moves forward during early times after exhalation
- Cloud: The distribution of ejected droplets that remain suspended even after the puff has lost its coherence. The cloud is advected by the air currents and is dispersed by ambient turbulence

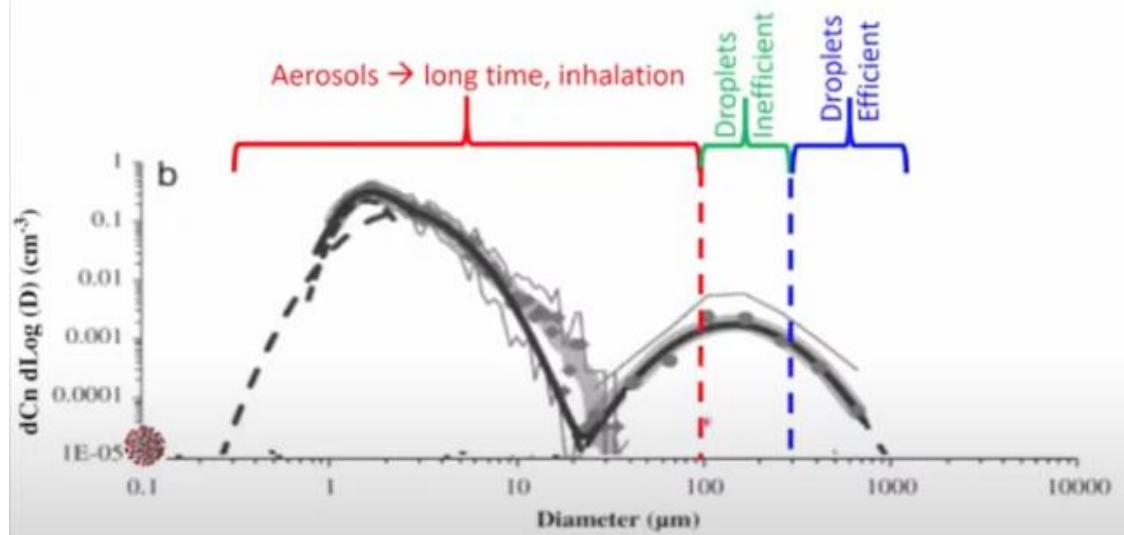
The three main stages involved in the host-to-host transmission of the virus: particle generation and emission during exhalation, airborne transport, and inhalation by the receiving host.

1. Emission of respiratory particles

In the generation stage, virus-laden drops are generated throughout the respiratory tract by the exhalation air flow, which carries them through the upper airway toward the mouth where they are ejected along with the turbulent puff of air from the lungs.

The ejected puff of air can be characterized with the following four parameters: the volume Q_{pe} , the momentum M_{pe} , and the buoyancy B_{pe} of the ejected puff, along with the angle θ_e to the horizontal at which the puff is initially ejected.

The ejected particles are characterized by their total number N_e , size distribution $N_e(d)$, particle velocity distribution $V_{de}(d)$ and particle temperature distribution $T_{de}(d)$, where d is the diameter of the respiratory particle.



2. Transport of respiratory particles

This is followed by the transport stage, where the initially ejected puff of air and droplets are transported away from the source. The volume of the puff of air increases due to entrainment of ambient air.

The puff velocity decreases due to both entrainment of ambient air as well as drag.

Since the temperature and moisture content of the ejected puff of air is typically higher than the ambient, the puff is also subjected to a vertical buoyancy force, which alters its trajectory from a rectilinear motion.

The exhaled puff is turbulent, and both the turbulent velocity fluctuations within the puff and the mean forward velocity of the puff decay over time.

To characterize the time evolution of the virus-laden droplets during the transport stage, we distinguish the droplets that remain within the puff, whose diameter is less than a cutoff (i.e., $d < d_{exit}$), from the droplets (i.e., $d > d_{exit}$) that escape out of the puff.

The *cutoff droplet size* d_{exit} decreases with time.

When the puff's mean and fluctuating velocities fall below those of the ambient, the puff can be taken to lose its coherence.

Thus, the puff remains coherent and travels farther in a confined relatively quiescent environment, such as an elevator, class room or aircraft cabin, than in an open outdoor environment with crosswind or in a room with strong ventilation.

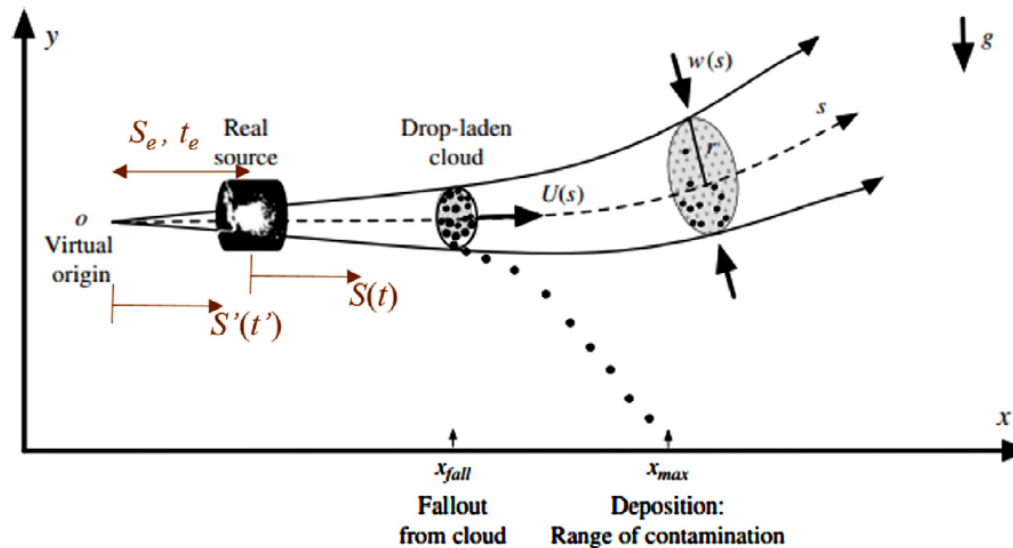


Fig. 6. Evolution of a typical cloud of respiratory multiphase turbulent droplet-laden air following breathing, talking, coughing and sneezing activities. Image adapted from Bourouiba et al. (2014).

Effect of non-volatiles

There can be significant presence of non-volatile material such as mucus, bacteria and bacterial products, viruses and fungi, and food debris in the ejected droplets.

However, the fraction of ejected droplet volume Q_{de} that is made up of these non-volatiles varies substantially from person to person.

The presence of non-volatiles alters the analysis of the previous sections in two significant ways. First, each ejected droplet, as it evaporates, will reach a final size that is dictated by the amount of non-volatiles that were initially in it. The larger the droplet size at initial ejection, the larger will be its final size after evaporation, since it contains a larger amount of non-volatiles. If ψ is the volume fraction of non-volatiles in the initial droplet, the final diameter of the droplet nuclei after complete evaporation of volatile matter (i.e., water) will be

$$d_{dr} = d_e \psi^{1/3}$$

This size depends on the initial droplet size and composition. Note that even a small, for example 1%, non-volatile composition results in d_{dr} being around 20% of the initial ejected droplet size.

It has also been noted that the evaporation of water can be partial, depending on local conditions in the cloud or environment.

We simply assume the fraction ψ to also account for any residual water retained within the droplet nuclei.

The second important effect of non-volatile is to reduce the rate of evaporation. As evaporation occurs at the droplet surface, a fraction of the surface will be occupied by the non-volatiles reducing the rate of evaporation.



3. Inhalation of respiratory particles

Depending on the location of the recipient host relative to that of the infected host, the recipient may be subjected to either the puff that still remains coherent, carrying a relatively high concentration of virus laden droplets or nuclei, or to the more dilute dispersion of droplet nuclei, or aerosols.

These factors determine the number and size distribution of virus-laden airborne droplets and nuclei the recipient host will be subjected to.

The inhalation cycle of the recipient, along with the use of masks and other protective devices, will then dictate the aerosols that reach sensitive areas of the respiratory tract where infection can occur.

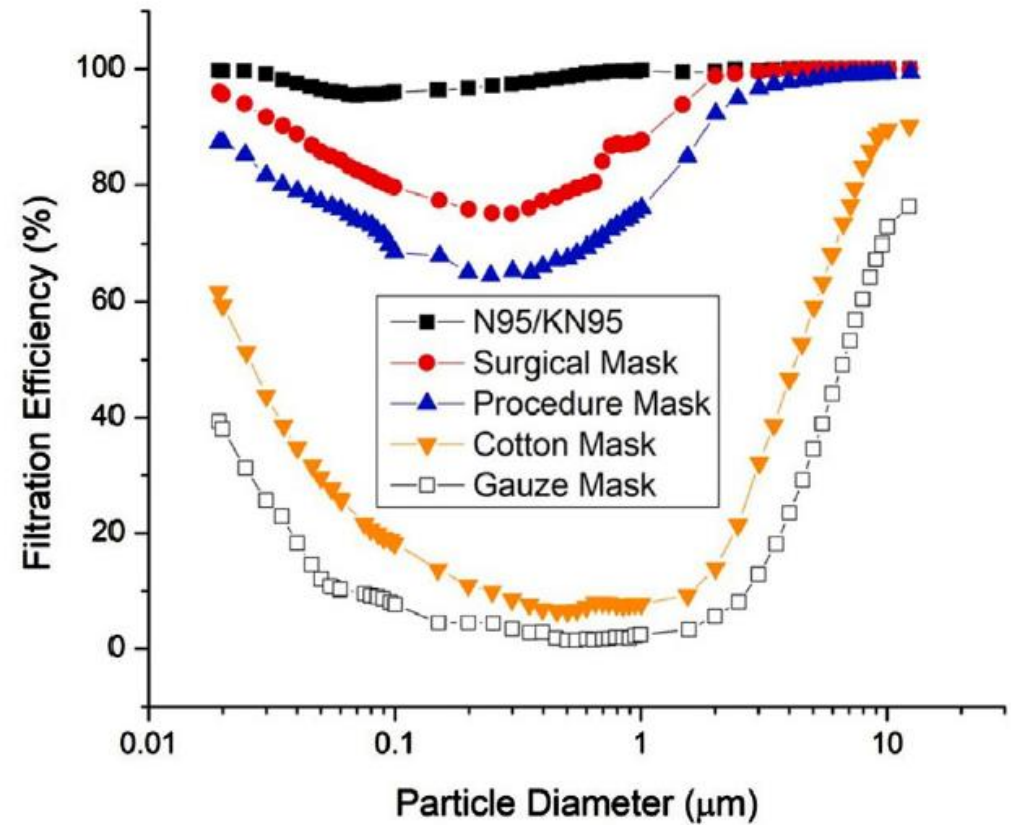
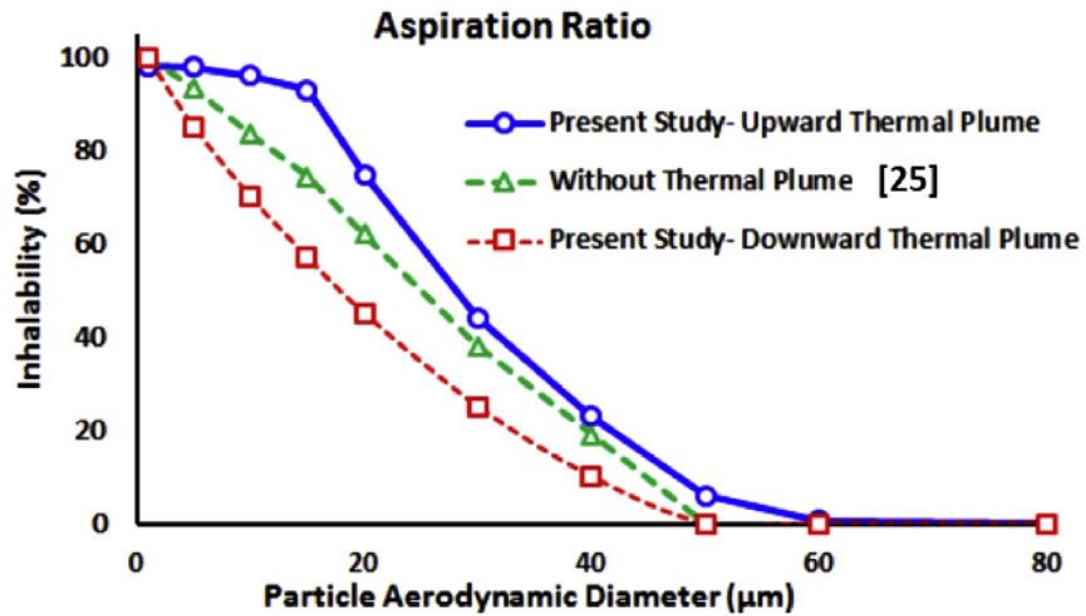


Fig. 11. Filtration efficiency of different respiratory masks under normal breathing conditions (Zhang et al., 2016; Feng et al., 2020).



ELSEVIER

Contents lists available at ScienceDirect

Science of the Total Environment

journal homepage: www.elsevier.com/locate/scitotenv

Effectiveness of commercial face masks to reduce personal PM exposure

A. Pacitto^{a,b}, F. Amato^{a,*}, A. Salmatoniadis^a, T. Moreno^a, A. Alastuey^a, C. Reche^a, G. Buonanno^{c,d,b}, C. Benito^e, X. Querol^a

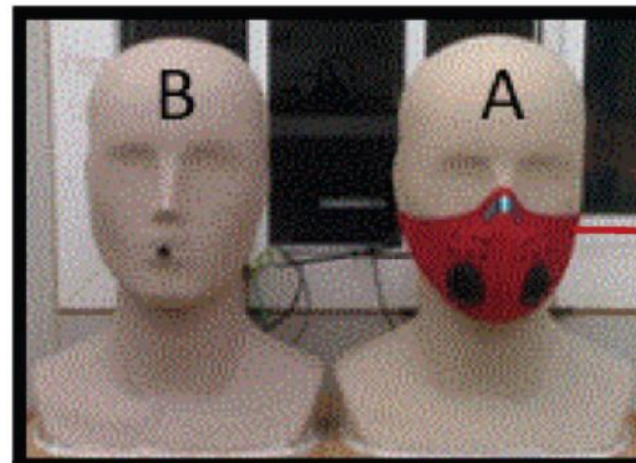
^a Institute of Environmental Assessment and Water Research (IDEA), Spanish National Research Council (CSIC), Barcelona, Spain

^b Department of Civil and Mechanical Engineering, University of Cassino and Southern Lazio, Cassino (FR), Italy

^c International Laboratory for Air Quality and Health, Queensland University of Technology, Brisbane, Australia

^d Department of Engineering, University "Parthenope", Naples, Italy

^e BACC, Bicicleta Club de Catalunya, Barcelona, Spain



PM _{2.5}	(-48%)	↓
LDSA	(-22%)	↓
BC	(-19%)	↓
UFP	(-19%)	↓

Cycling and walking are promoted as means of transportation which can contribute to the reduction of traffic pollution in urban areas. However, cyclists and pedestrians may be exposed to high concentrations of air pollutants due to their proximity to vehicle emissions. Commercial face mask respirators are widely used, in both developing and developed countries, as an individual protective measure against particle pollution. However scientific data on the efficacy of face mask respirators in reducing airborne particle exposure is limited. In this study, a custom experimental set-up was developed in order to measure the effectiveness of nine different respirators under real environmental conditions in terms of particle mass concentration below 2.5 μm (PM_{2.5}), particle number concentration (PNC), Lung Deposited Surface Area (LDSA) and Black Carbon concentration (BC). Face mask performances were assessed in a typical traffic affected urban background environment in the city of Barcelona under three different simulated breathing rates to investigate the influence of flow rate. Results showed a median face mask effectiveness for PM_{2.5} equal to 48% in a range of 14–96%, 19% in a range of 6%–61% for BC concentration, 19% in a range of 4%–63% for PNC and 22% in a range of 5%–65% for LDSA. For each pollutant under investigation, the best performance was found always with the same mask (N7) although it is not the most expensive (in a range of price of 1 to 44, its cost was 20 euros), which has a filter on the entire surface except for the 2 exhalation valves where air cannot enter but just exit and shows a good fit on the dummy head.

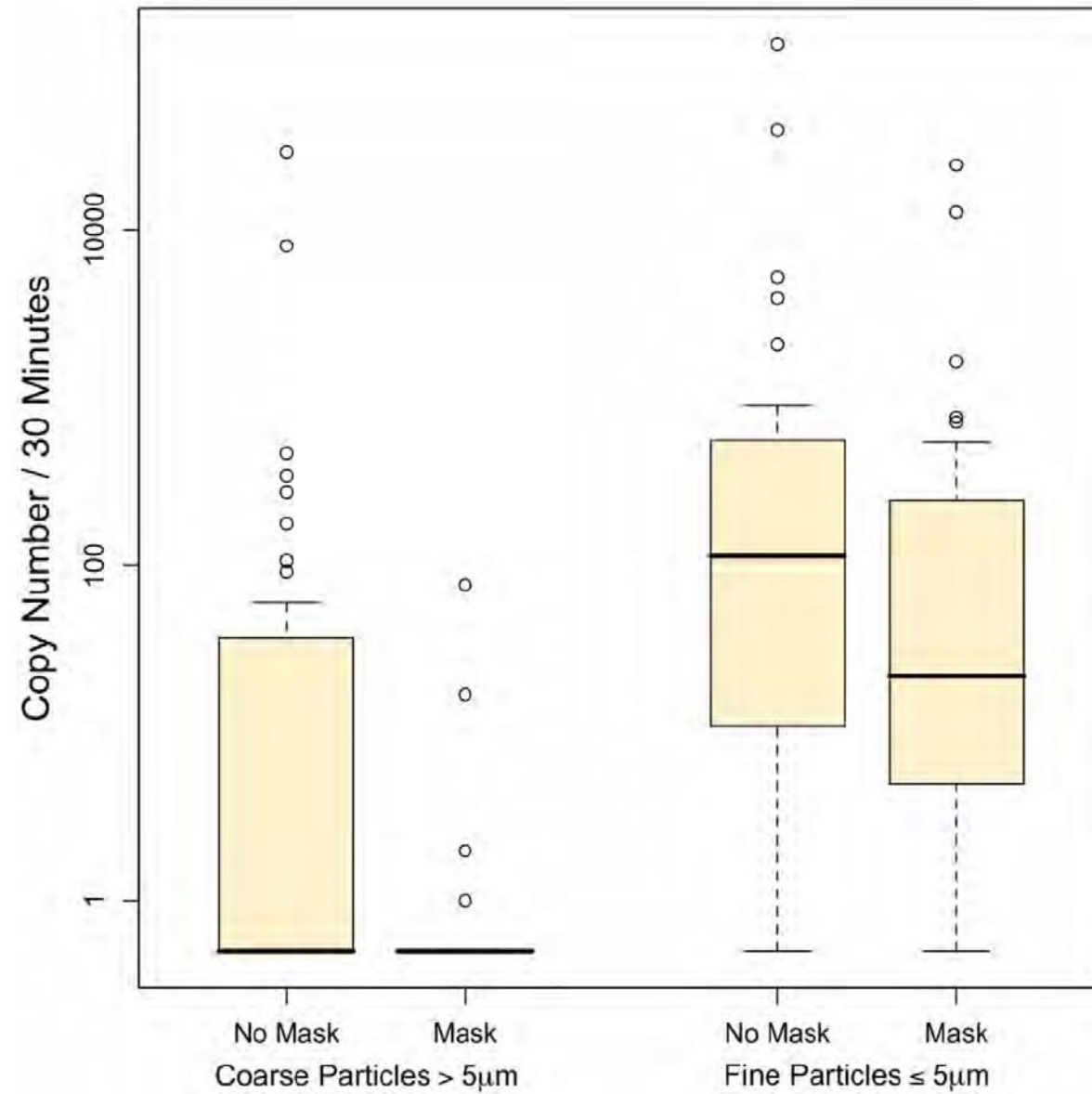


Figure 1. Influenza virus copy number in aerosol particles exhaled by patients with and without wearing of an ear-loop surgical mask. Counts below the limit of detection are represented as 0.5 on the log scale.
doi:10.1371/journal.ppat.1003205.g001



Contents lists available at ScienceDirect

Science of the Total Environment

journal homepage: www.elsevier.com/locate/scitotenv



Close proximity risk assessment for SARS-CoV-2 infection

G. Cortellessa^a, L. Stabile^a, F. Arpino^a, D.E. Faleiros^b, W. van den Bos^b, L. Morawska^c, G. Buonanno^{a,c,*}

^a Department of Civil and Mechanical Engineering, University of Cassino and Southern Lazio, Cassino, FR, Italy

^b Maritime and Transport Technology, TU Delft, Netherlands

^c International Laboratory for Air Quality and Health, Queensland University of Technology, Brisbane, Qld, Australia



An integrated risk assessment is presented for SARS-CoV-2 close contact exposure between a speaking infectious subject and a susceptible subject;

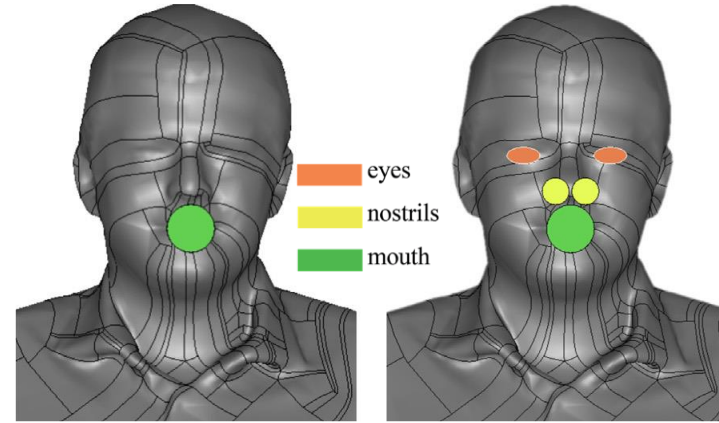
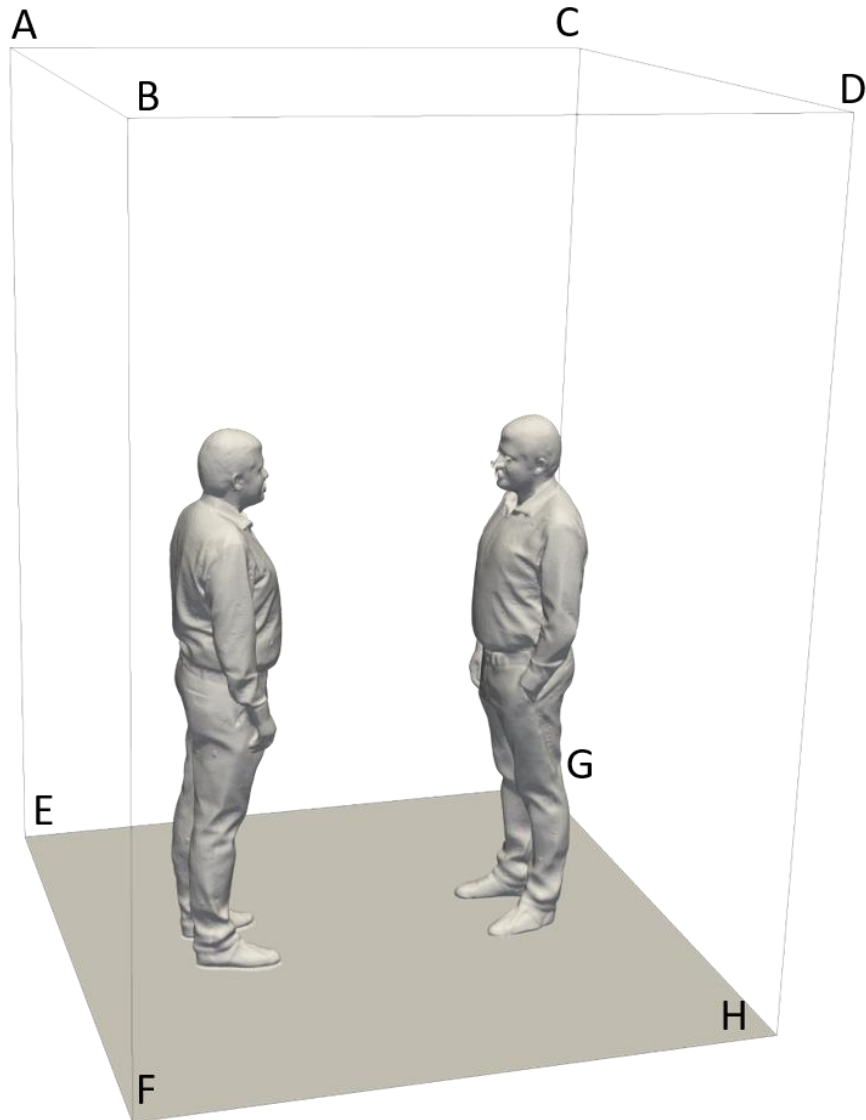
It is based on a three-dimensional transient numerical model for the description of exhaled droplet spread once emitted by a speaking person, coupled with a recently proposed SARS-CoV-2 emission approach;

Particle Image Velocimetry (PIV) measurements were conducted to validate the numerical model;

The contribution of large droplets to infection risk is dominant for distances < 0.6 m, whereas for longer distances, the exposure risk depends only on airborne droplets.

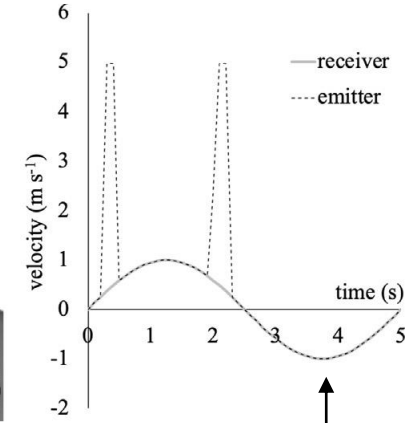
Based on the interpersonal distances across countries reported as a function of interacting individuals, cultural differences, and environmental and sociopsychological factors, the approach presented here revealed that, in addition to intimate and personal distances, particular attention must be paid to exposures longer than 1 min within social distances (of about 1 m).

Computational domain and boundary conditions



Emitter *Receiver*

Schematization of the surfaces of interest for emitter and receiver (eyes, nostrils, and mouth)



the transient velocity profile adopted as a boundary condition at the emitter and receiver mouths

Boundary conditions (BC) adopted for the external surfaces of the computational domain and for the subjects.

Surface	BC for velocity	BC for pressure	BC for temperature
ABEF	$\mathbf{u} = 0$	$\frac{\partial p}{\partial n} = 0$	$\frac{\partial T}{\partial n} = 0$
CDGH	$\mathbf{u} = 0$	$\frac{\partial p}{\partial n} = 0$	$\frac{\partial T}{\partial n} = 0$
BDFH	$\mathbf{u} = 0$	$\frac{\partial p}{\partial n} = 0$	$\frac{\partial T}{\partial n} = 0$
ACEG	$\mathbf{u} = 0$	$\frac{\partial p}{\partial n} = 0$	$\frac{\partial T}{\partial n} = 0$
ABCD	$\frac{\partial \mathbf{u}}{\partial n} = 0$	$p = 101325 \text{ Pa}$	$T = 293.15 \text{ K}$
Emitter mouth	See Figure	$\frac{\partial p}{\partial n} = 0$	$T = 308.15 \text{ K}$
Receiver mouth	$\mathbf{u} = A \cdot \sin(2\pi ft)$	$\frac{\partial p}{\partial n} = 0$	$T = 308.15 \text{ K}$

Numerical model: Eulerian-Lagrangian approach

One-way coupling between continuum and discrete phase

Assumptions:

- 3D
- Unsteady
- Turbulent
- Compressible
- Ideal gas behavior
- RANS approach for turbulence modeling → Shear Stress Transport (SST) k - ω model, Standard Wall Functions

- Newton's equation of motion is solved for each particle (discrete phase)

Assumptions:

- Elastic collision among particles

Mathematical-numerical model: Lagrangian Particle Tracking (LPT)

The airborne droplets motion has been described solving the following equations:

$$m_d \frac{d\mathbf{u}_d}{dt} = \mathbf{F}_D + \mathbf{F}_g \quad (1)$$

$$\frac{d\mathbf{x}_d}{dt} = \mathbf{u}_d \quad (2)$$

$$F_D = m_d \frac{18}{\rho_d \cdot d_d^2} C_D \frac{Re_d(\mathbf{u} - \mathbf{u}_d)}{24} \quad (3)$$

$$Re_d = \frac{\rho(|\mathbf{u} - \mathbf{u}_d|)d_d}{\mu} \quad (4)$$

$$C_D = \begin{cases} \frac{24}{Re_d} & \text{if } Re_d < 1 \\ \frac{24}{Re_d} (1 + 0.15 \cdot Re_d^{0.687}) & \text{if } 1 \leq Re_d \leq 1000 \\ 0.44 & \text{if } Re_d > 1000 \end{cases} \quad (5)$$

m_d (kg): mass of the droplet;

\mathbf{u}_d ($\frac{m}{s}$): droplet velocity;

t (s): time;

\mathbf{F}_D (N): drag force;

\mathbf{F}_g (N): gravity force;

\mathbf{x}_d (m): trajectory of the droplet;

ρ_d ($\frac{kg}{m^3}$): droplet density, considered constant and equal to 1200 kg·m⁻³;

d_d (m): diameter of the droplet;

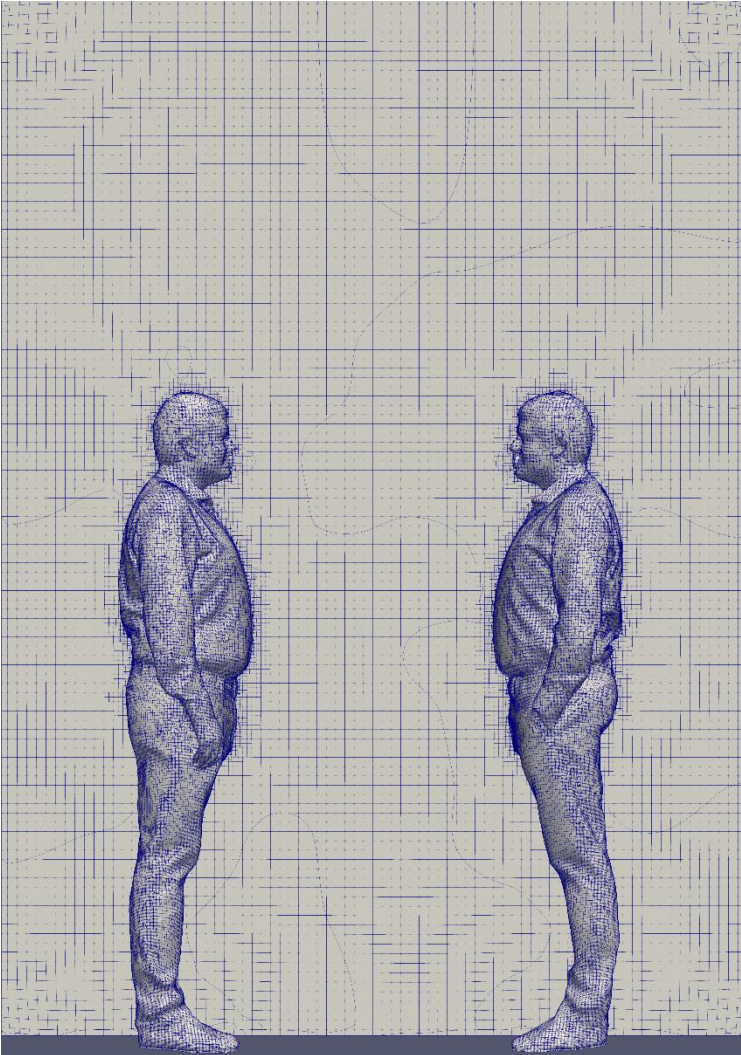
C_D : drag coefficient;

Re_d : Reynolds number of the droplet;

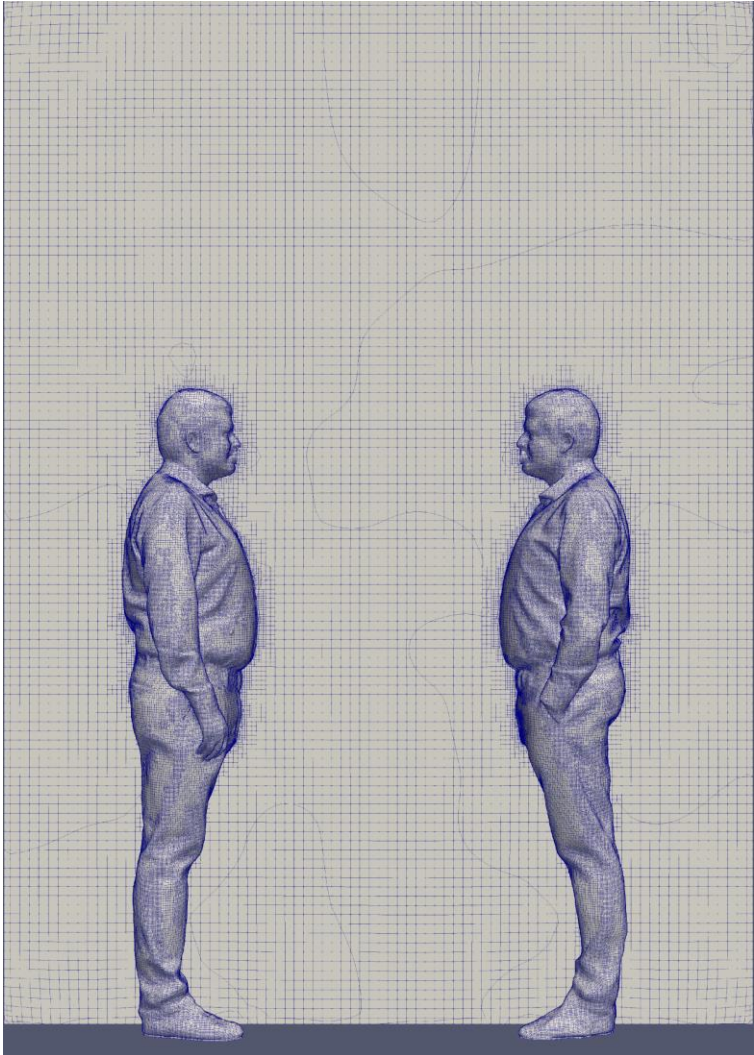
\mathbf{u} ($\frac{m}{s}$): air velocity;

ρ ($\frac{kg}{m^3}$): air density.

Computational grid sensitivity analysis



Computational grid composed by 425440 cells



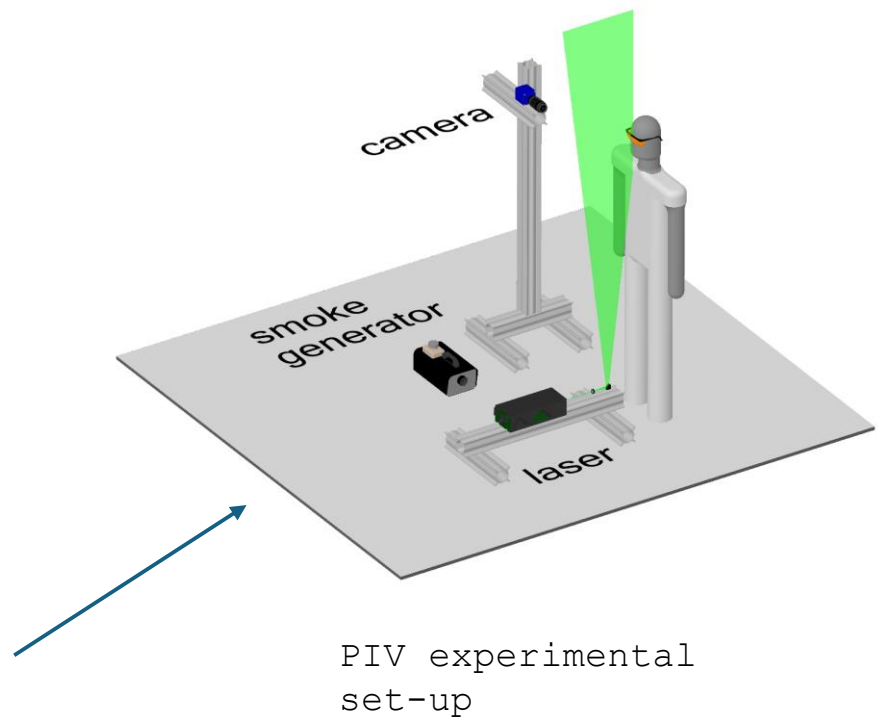
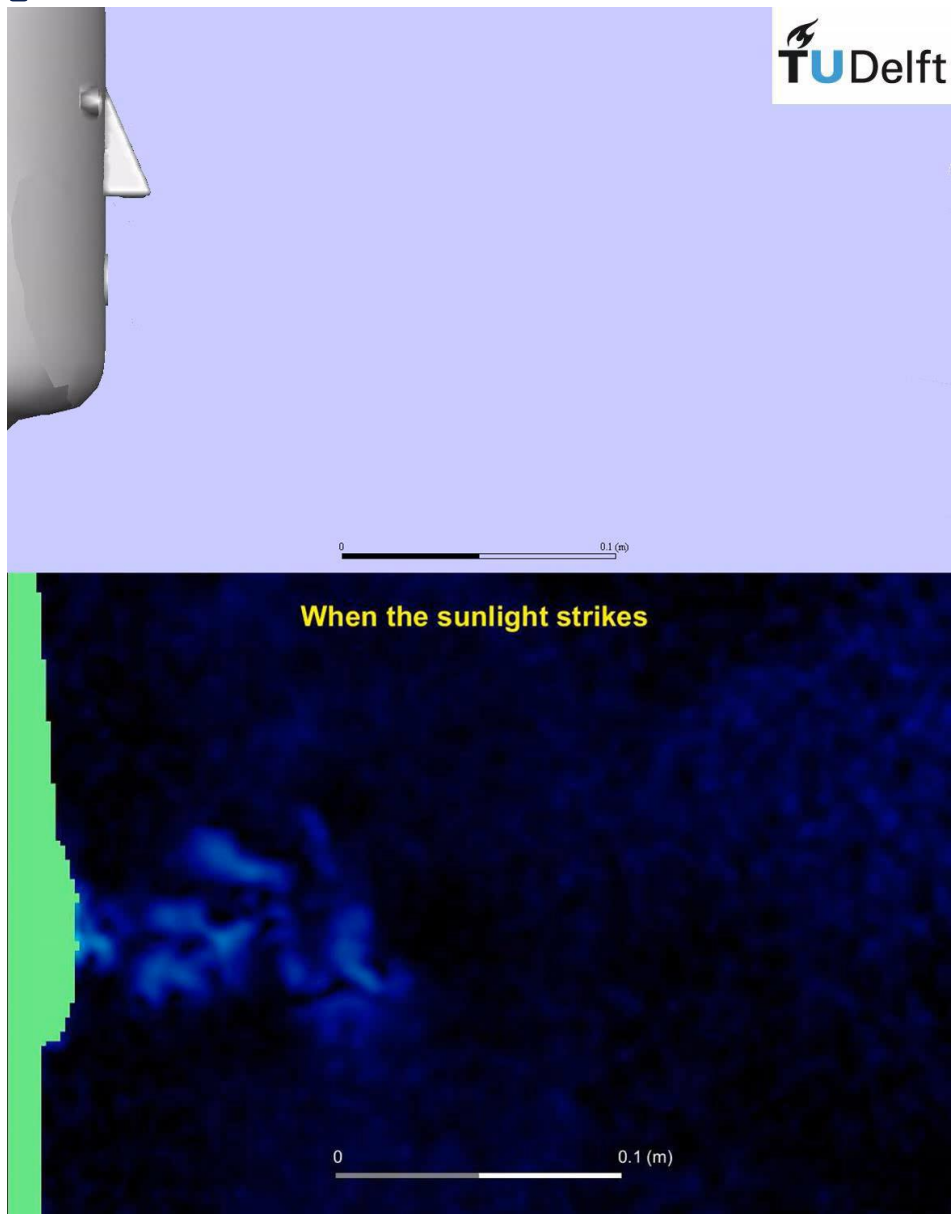
Computational grid composed by 1287642 cells

Droplets number and volume distribution

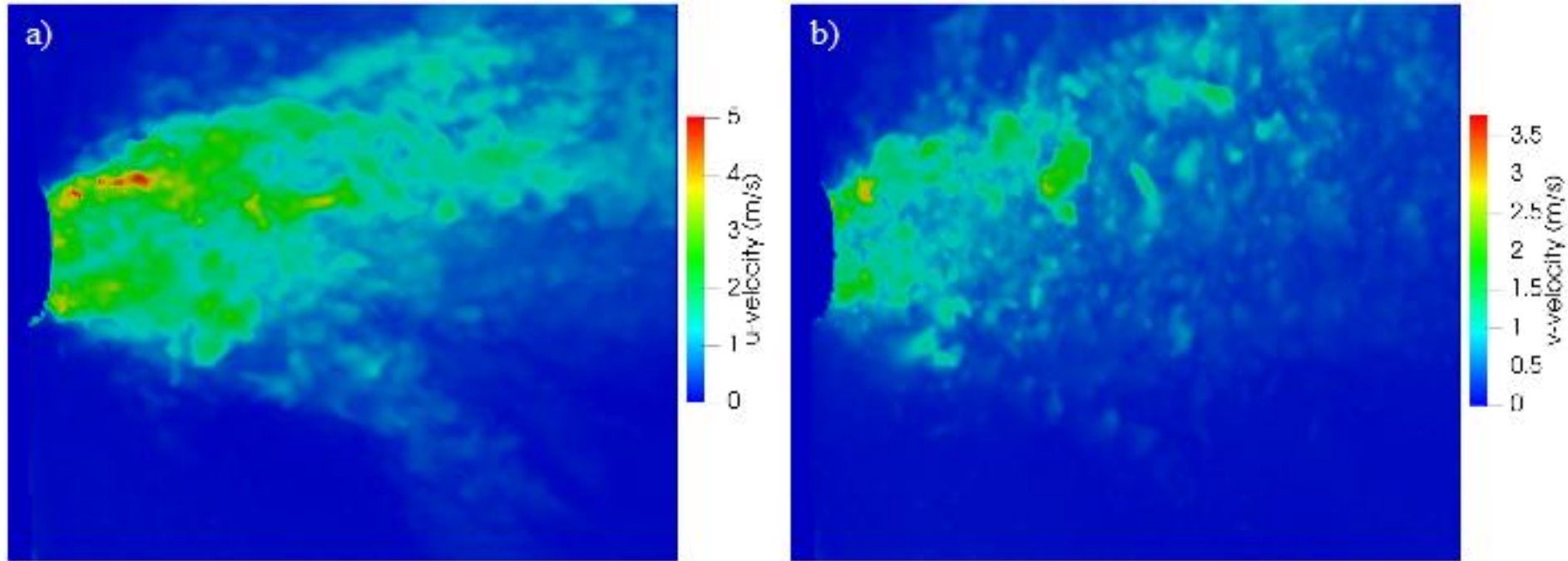
Type of droplets	Pre-evaporation					Post-evaporation		
	Droplet diameter, d_a (μm)	$dN/d\log(d_a)$ (droplet cm^{-3})	$dV/d\log(d_a)$ ($\mu\text{L cm}^{-3}$)	ER_N (droplet s^{-1})	ER_V ($\mu\text{L s}^{-1}$)	Droplet diameter, d_a (μm)	$dN/d\log(d_a)$ (droplet cm^{-3})	$dV/d\log(d_a)$ ($\mu\text{L cm}^{-3}$)
Respiratory droplets	4.6 μm (< 0.5 to 4.6 μm)	0.266	1.39×10^{-10}	217.6	1.14×10^{-7}	1 μm (< 1 μm)	0.266	1.39×10^{-8}
	9.0 μm (4.6 to 17.7 μm)	0.035	1.33×10^{-10}	20.3	7.80×10^{-8}	1.9 μm (1.0 to 3.8 μm)	0.035	1.33×10^{-8}
	23.2 μm (17.7 to 30.4 μm)	0.013	8.74×10^{-10}	3.1	2.05×10^{-7}	5 μm (3.8 to 6.6 μm)	0.013	8.74×10^{-8}
	45.5 μm (30.4 to 68.2 μm)	0.016	8.08×10^{-9}	5.7	2.83×10^{-6}	9.8 μm (6.6 to 14.7 μm)	0.016	8.08×10^{-7}
	78 μm (68 to 90 μm)	0.015	3.83×10^{-8}	1.8	4.48×10^{-6}	16.8 μm (14.7 to 19.2 μm)	0.015	3.83×10^{-6}
Large droplets	100 μm (90 to 120 μm)	0.014	7.09×10^{-6}	1.6	8.29×10^{-4}	100 μm (90 to 120 μm)	0.014	7.09×10^{-6}
	300 μm (120 to 800 μm)	0.005	6.53×10^{-5}	4.3	6.11×10^{-2}	300 μm (120 to 800 μm)	0.005	6.53×10^{-5}
Total		0.254	6.27×10^{-5}	254.5	6.19×10^{-2}		0.254	6.19×10^{-5}

Droplet number and volume distributions pre- and post-evaporation (fitted by seven size ranges) adopted in the simulations. Droplet diameters and corresponding ranges before and after evaporation are also reported, as well as droplet number and volume emission rates. Airborne and large droplets were separately identified.

Numerical model validation: comparison between numerical and experimental results

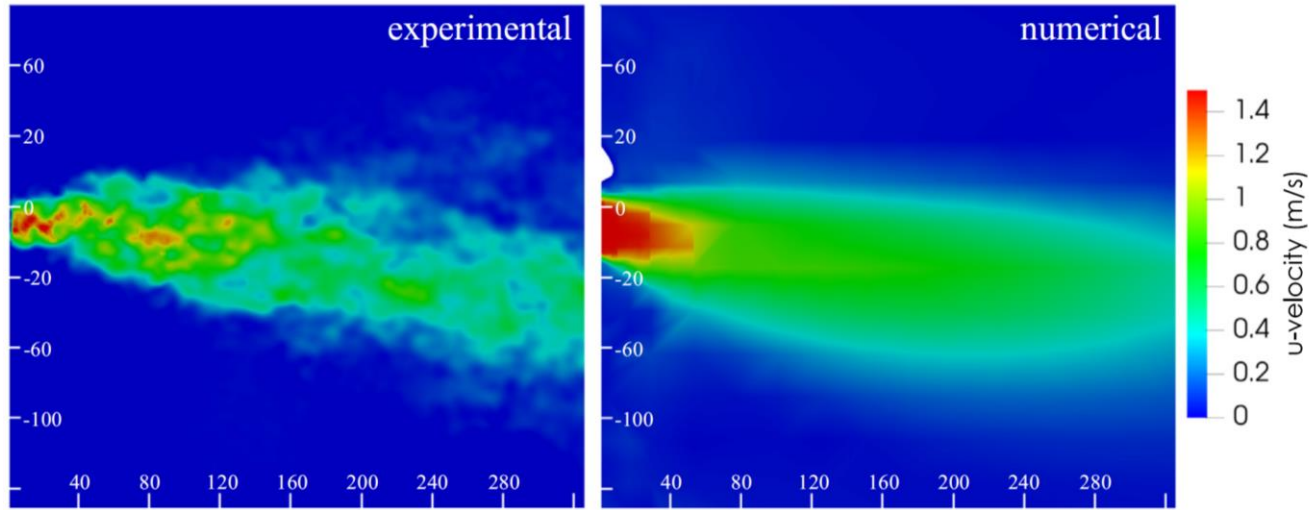


Experimental results detail obtained by Particle Image Velocimetry

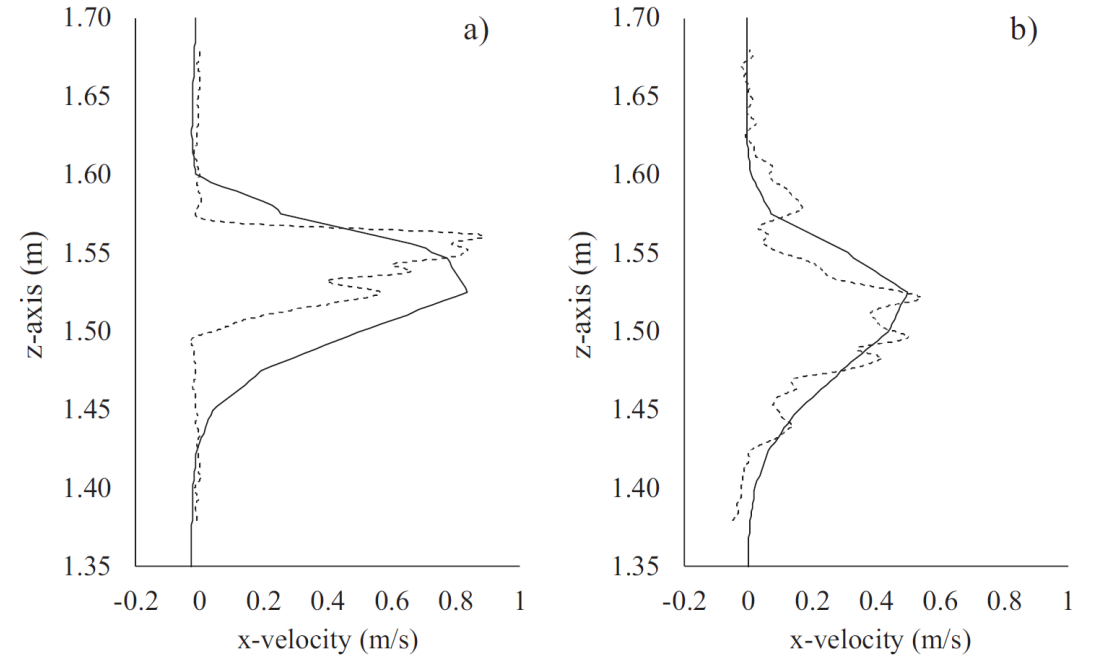


Instantaneous u-velocity (a) and v-velocity (b) contours obtained by particle image velocimetry during reading of the excerpt from the rainbow passage.

Numerical model validation by Particle Image Velocimetry

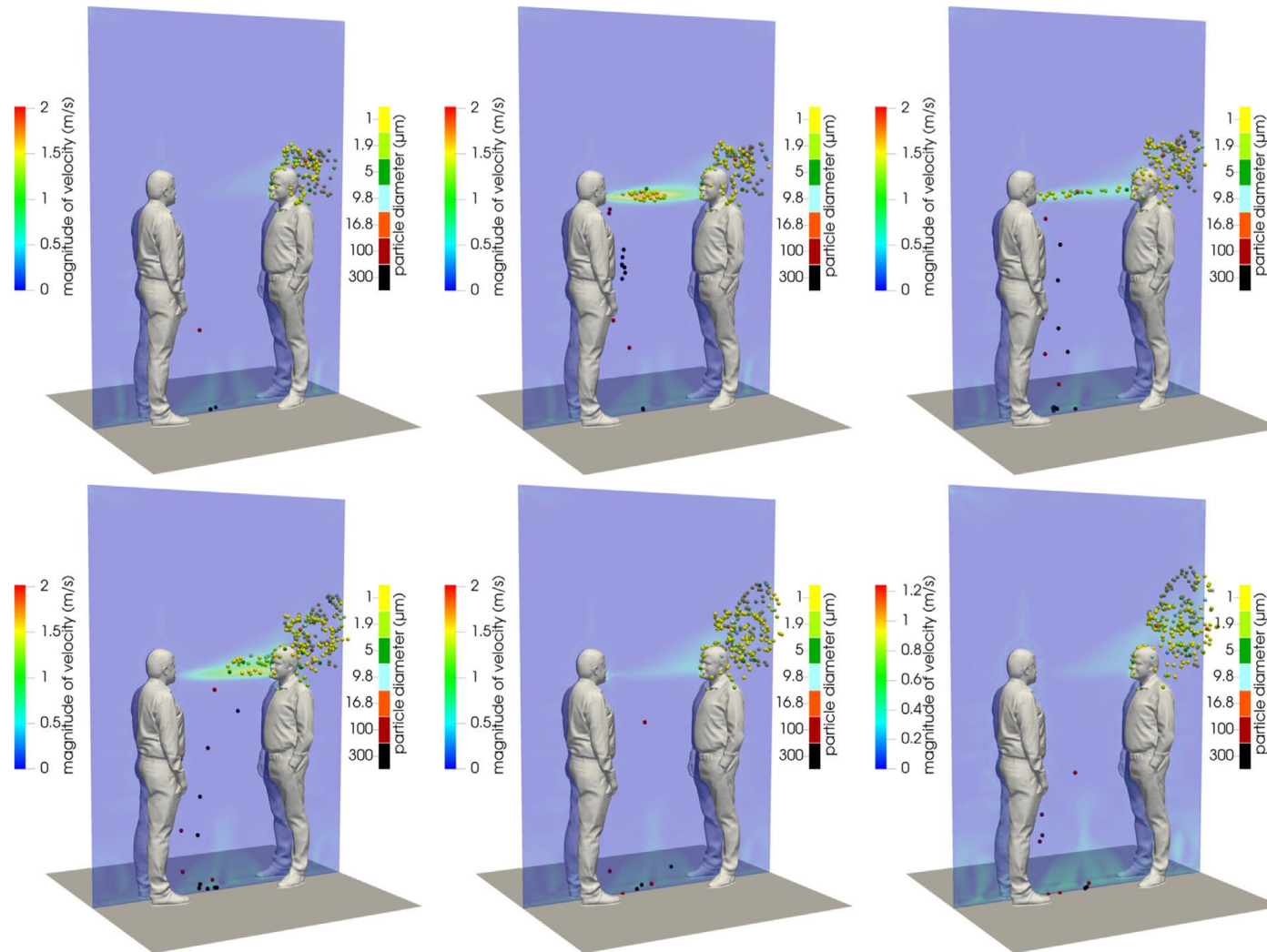


Experimental and CFD velocity contours obtained in a sagittal plane by synchronizing the instant of time for breathing at which the maximum velocity values are reached.



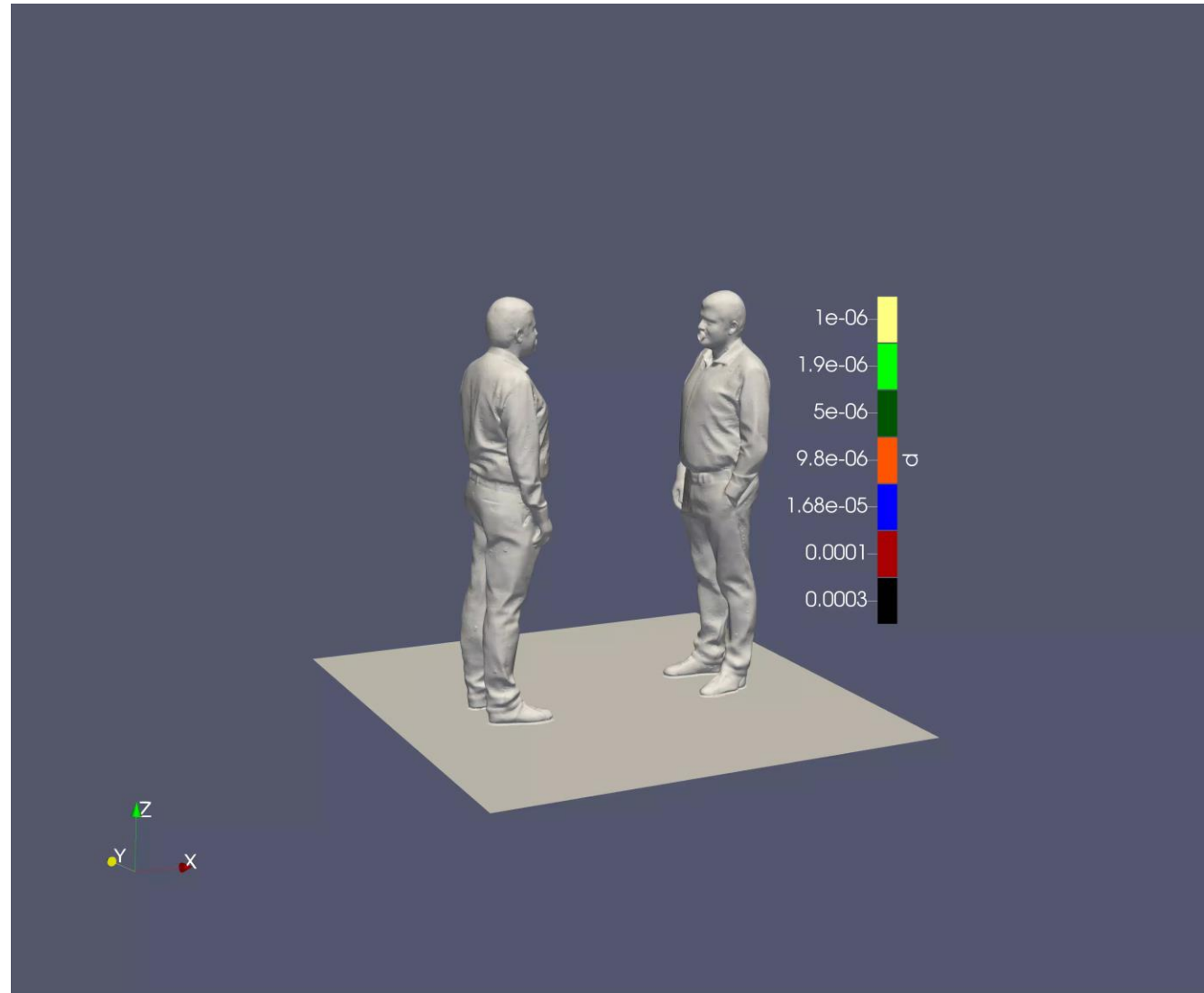
Experimental (particle image velocimetry, dotted lines) and CFD (solid lines) velocity profile comparison obtained in a sagittal plane at a distance from the emitter mouth equal to 0.10 m (a) and 0.32 m (b).

Numerical model: particle emission dynamics

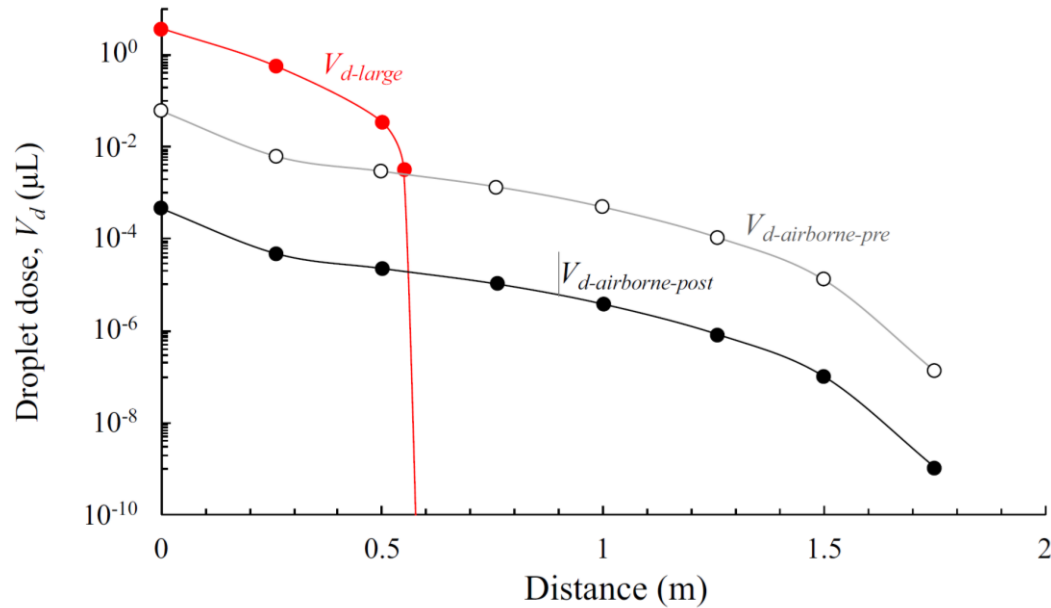


Numerical velocity contours during a single breath at a distance of 0.76 m between people: six selected computational times (5, 5.5, 6.5, 7.5, 8.5, and 10 s) are shown.

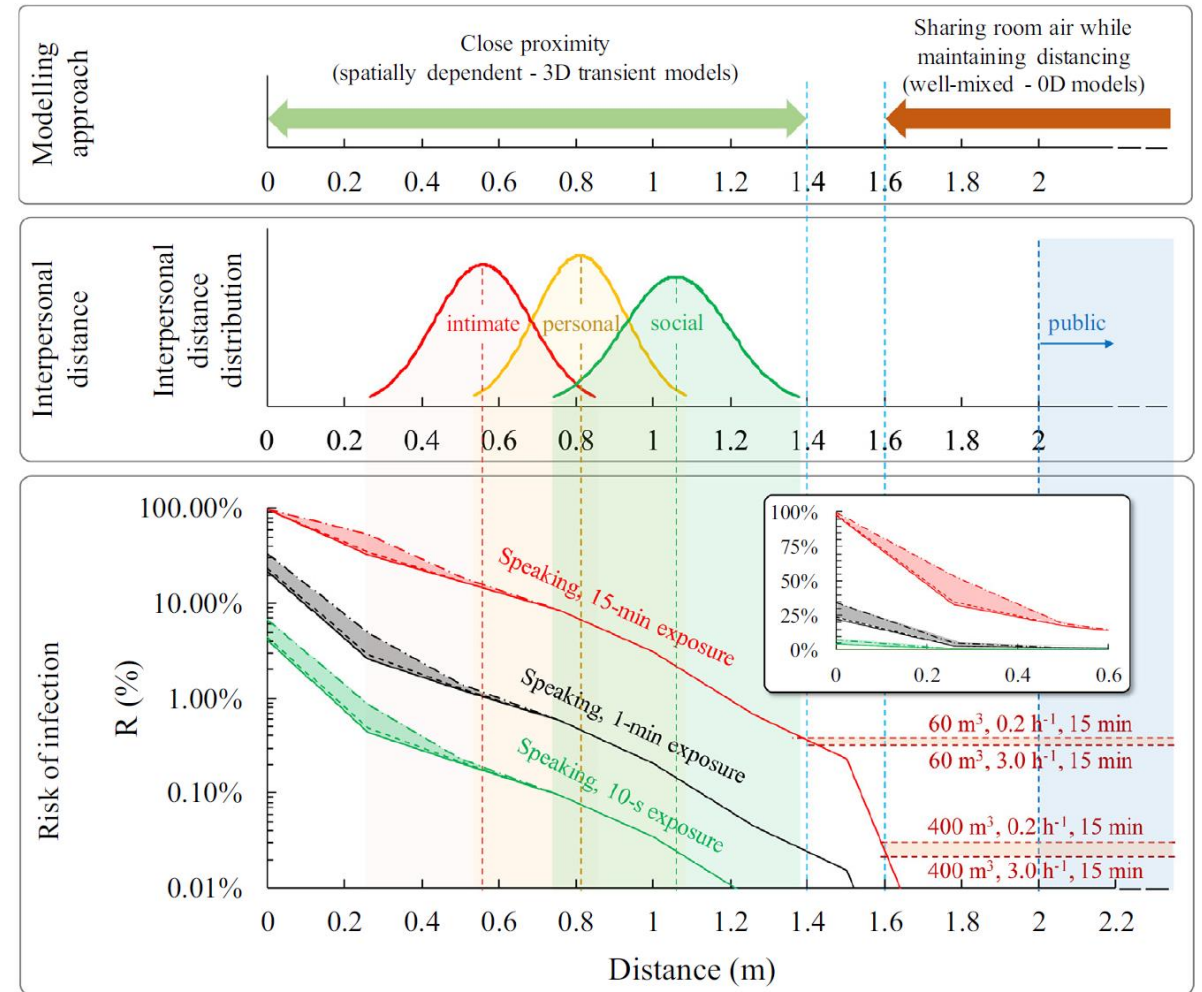
Animation of particle emission dynamics



Risk assessment of Sars-Cov-2 infection



1-min large ($V_{d\text{-large}}$) and airborne droplet doses ($V_{d\text{-airborne-pre}}$ and $V_{d\text{-airborne-post}}$) received by the susceptible subject (by deposition and inhalation, respectively) as a function of the distance between the two subjects



Infection risk (R , %) of a susceptible subject as a function of the time of exposure and interpersonal distance from the infected subject; infection risk trends at short and long distances are highlighted as well as the modeling approaches to be applied.

Received: 16 June 2020

Revised: 26 August 2020






Accepted: 15 September 2020

DOI: 10.1111/ina.12751

ORIGINAL ARTICLE

WILEY

Transmission of SARS-CoV-2 by inhalation of respiratory aerosol in the Skagit Valley Chorale superspreading event

Shelly L. Miller¹  | William W Nazaroff²  | Jose L. Jimenez³  | Atze Boerstra⁴ |
Giorgio Buonanno⁵ | Stephanie J. Dancer⁶ | Jarek Kurnitski⁷ | Linsey C. Marr⁸  |
Lidia Morawska⁹  | Catherine Noakes¹⁰

A super spreading event (SSE) occurred in Skagit Valley, Washington, USA. When the Skagit Valley Chorale (SVC) met on the evening of March 10, 2020, one person attending the rehearsal had cold-like symptoms that had developed 3 days earlier; that individual subsequently tested positive for COVID-19.

At the time of the rehearsal, the Skagit County Health Department was not recommending widespread closure of public venues or public events. They were recommending that those 60 years of age and older, or persons with underlying medical conditions, should avoid large public gatherings.

Choral members were told to not attend on March 10 if they were sick with any kind of symptoms or if they had concerns.

The chorale met in the Fellowship Hall of a church in Mount Vernon, Skagit County. The day after the rehearsal on March 11, the governor of Washington recommended physical distancing and no large group meetings in three other nearby counties. At the time of the rehearsal, there were no known COVID-19 cases in Skagit County, nor were any closures in effect.

The SVC has 122 members, but only 61 attended rehearsal on March 10, amid concerns about COVID-19 transmission.

Precautions were taken during rehearsal, including the use of hand sanitizer, no hugging, and no handshakes.

All 120 chairs were arranged by 3 people who arrived early, and members sat in their usual chairs, which increased their distance compared to other well-attended rehearsals. Lateral distance between chair centers (and thus nose/ mouth distances) was ~0.75 m, while forward distance between rows was ~1.4 m.



MONT VERNON

REGULARE ANGEBORE
VERKLEINERUNG

Some members began experiencing illness from March 11 to March 22.

The timing of these potential secondary infections is consistent with what is known about the temporal dynamics of virus shedding and serial interval for COVID-19.

Among the 61 attendees at the rehearsal, 53 cases in total were subsequently identified including the index case, with 33 confirmed through positive COVID-19 tests and 20 unconfirmed but probable secondary cases based on symptoms and timing.

The large number of infections arising from this event, compared to the low incidence in the county at the time, makes it unlikely that they were acquired at a different setting than the choir.

A seating chart obtained through personal communication

showed the layout of participants among 120 chairs plus the position of the choir director and piano accompanist. Although the chart cannot be reproduced because of privacy concerns, a centrally important point for interpreting the cause of transmission is that the cases occurred throughout the room with no clear spatial pattern.

The rehearsal started at 6:30 PM and ended at 9:00 PM.

The Fellowship Hall is heated and ventilated with a mechanical air heating system including an outdoor air intake and air recirculation. It is not known how much outside make-up air was supplied to the building that evening. The furnace is also outfitted with a MERV 11 filter, which has a rated single-pass efficiency of $\geq 30\%$ -65% for aerosol particles of diameter 1 μm or larger.

During the entire rehearsal no exterior doors were open. It is not known whether the forced-air furnace fan operated (only) under thermostatic control or whether it ran continuously.

A well-mixed material balance model for the room (Equation 2) is applied next to relate the quanta concentration, C (quanta/m³), to the emission rate, E (quanta/h):

$$\frac{dC}{dt} = \frac{E}{V} - \lambda C \quad (2)$$

Here V = volume of the rehearsal hall (m³) and λ = first-order loss rate coefficient for quanta (h⁻¹) due to the summed effects of ventilation (λ_v), deposition onto surfaces (λ_{dep}), and virus decay (k).⁵⁴ Assuming the quanta concentration is 0 at the beginning of the rehearsal, Equation (2) is solved and the average concentration determined as follows (Equation 3):

$$C(t) = \frac{E}{\lambda V} (1 - e^{-\lambda t}) \quad (3)$$

$$C_{avg} = \frac{1}{D} \int_0^D C(t) dt = \frac{E}{\lambda V} \left[1 - \frac{1}{\lambda D} (1 - e^{-\lambda D}) \right] \quad (4)$$

Here, t = time (h). Equation (4) is rearranged to solve for the emission rate, E :

$$E = \lambda V C_{avg} \left[1 - \frac{1}{\lambda D} (1 - e^{-\lambda D}) \right]^{-1} \quad (5)$$

FIGURE 2 Probability of infection as a function of loss rates for varying event duration (D, h). A mean emission rate (970 q/h) and constant volumetric breathing rates of 1.0 m³/h were assumed

